Nanoscale

PAPER

View Article Online
View Journal | View Issue

Cite this: *Nanoscale*, 2025, **17**, 7837

Fluffy mesoporous Al_2O_3 supported Ag–In_2O_3 schottky junction catalysts for selective hydrogenation of C=O of α,β-unsaturated aldehydes†

Jiasheng Wang, *[a,b] Tianyu Zhang,[a,b] Jiliang Song,[a,b] Fengxin Zhang,[a,b] Hong Liu,[a,b] Wan-Hui Wang [a,b] and Ming Bao *[a,b]

Received 31st December 2024,
Accepted 19th February 2025

DOI: 10.1039/d4nr05518g

rsc.li/nanoscale

Unsaturated alcohols (UOLs) are important fine chemical intermediates. Thus, it is of great significance to design and prepare catalysts for highly selective hydrogenation of C=O of α,β-unsaturated aldehydes (UALs). In this paper, a fluffy mesoporous Al_2O_3-supported Ag–In_2O_3 catalyst (Ag-In_2O_3/*f*-*m*-Al_2O_3) was synthesized by employing a two-solvent method, in which Ag and In_2O_3 form a Mott–Schottky junction and lead to electron transfer from In_2O_3 to Ag. Electron-rich Ag repels the C=C bond owing to "four-electron repulsion", and electron-deficient In_2O_3 acts as the electrophilic site to adsorb the O atom of the C=O bond, thus improving the selectivity towards UOLs. In addition to a larger specific surface area and smaller mass transfer resistance, the fluffy mesopore Al_2O_3 exhibits a large number of Lewis acid sites, which can further improve UOL selectivity. With the help of Ag–In_2O_3/*f*-*m*-Al_2O_3, high UOL selectivity can be obtained from UALs containing aliphatic, aromatic and heterocyclic groups. This elaborate design of the catalyst could contribute to the highly selective hydrogenation of UALs to UOLs.

[a]*State Key Laboratory of Fine Chemicals, Dalian University of Technology, Dalian, 116024, China. E-mail: jswang@dlut.edu.cn, mingbao@dlut.edu.cn*
[b]*School of Chemical Engineering, Ocean and Life Sciences, Dalian University of Technology, Panjin, 124221, China*

† Electronic supplementary information (ESI) available. See DOI: https://doi.org/10.1039/d4nr05518g

Jiasheng Wang

Jiasheng Wang is currently an Associate Professor in the School of Chemical Engineering, Ocean and Life Sciences, at the Dalian University of Technology (DUT). He received his BS at DUT in 2004 and then worked at Asymchem Inc. until 2007. He obtained his PhD from DUT in 2014 and then held an appointment there. His research interests lie in the synthesis and application of novel nanocatalytic materials in selective hydrogenation and oxidation reactions. Besides a series of ultrasmall heterojunction catalysts for the hydrogenation of CO_2, fatty acids/esters, halogenated nitroarenes, and unsaturated aldehydes with high activity and selectivity, his group also developed promising catalysts for the oxidation of thiophenes, aromatics, and alkenes.

1. Introduction

Unsaturated alcohols (UOLs), as important organic intermediates, are widely used to synthesize organic chemicals, such as resins, spices, medicines, surfactants and food additives.[1–3] Selective hydrogenation of α,β-unsaturated aldehydes (UALs) is one of the important methods to prepare unsaturated alcohols.[4–6] However, because the activation energy of the C=C bond is lower than that of the C=O bond, it is difficult to achieve the preferential hydrogenation of the C=O bond.[7–9]

To achieve the selective hydrogenation of the C=O bond, it is necessary to design catalysts that can inhibit the hydrogenation of the C=C bond and promote the hydrogenation of the C=O bond.[10–13] The adsorption mode of UALs determines the selectivity of the product. According to Delbecq and Sautet's work,[14,15] there are nine possible adsorption modes for UALs on the catalyst surface, as shown in Fig. S1.† Among them, the η_2 diσ_{CO} adsorption mode, in which the C and O of the C=O bond are simultaneously adsorbed, is considered the best adsorption mode for the selective hydrogenation of UALs to UOLs.

Because the C=O bond is a polar bond, to realize the η_2 diσ_{CO} adsorption mode, catalysts with both electrophilic and nucleophilic sites are more advantageous.[16] Therefore, frustrated Lewis pairs (FLPs) with Lewis acids and bases,

which fail to form classical Lewis acid–base sites owing to steric hindrance, have been used in recent years to catalyse this reaction to obtain high selectivity but usually need complex procedures.[17–19] Theoretically, catalysts with oppositely charged sites can also simultaneously adsorb C and O of C=O and meanwhile induce heterolysis of hydrogen to polar active hydrogen ions, which is conducive to the hydrogenation of polar C=O bonds.[20–22] Therefore, bimetallic catalysts have drawn much attention, where platinum group metals (PGMs) with high electronegativity are often needed.[23–26] To avoid the use of expensive PGMs,[27,28] Schottky junctions (M-MO_X) formed by the contact and electron transfer between metals and semiconductors (such as metal oxides) have become an ideal candidate owing to their oppositely charged components.[29] Among the two types of Schottky junctions, metal–n-type semiconductors and metal–p-type semiconductors, the former is a better choice because it can create an electron-enriched metal centre *via* electron transfer from the n-type semiconductor to the active metal.[30] The electron-enriched active metal strengthens the four-electron repulsion to C=C.[31,32] Meanwhile, the electron-deficient metal oxide serves as an electrophilic site promoting C=O adsorption.[33] For metal–p-type semiconductor Schottky catalyst without such a repulsion, the hydrogenation of the C=C bond is preferential, as reported by Ren *et al.*[34]

Ag was chosen as the active metal because it has shown unique high selectivity for C=O bond hydrogenation of UAL.[35–37] Tian *et al.* also found that Ag had a good adsorption and activation effect on the C=O bond.[38] In_2O_3 was chosen as the promoter because it is a typical n-type semiconductor that is easy to donate electrons.[30,39–41]

Theoretically, Lewis acidic support can improve the selectivity of C=O owing to the electrophilicity of the empty orbitals.[42] Thus, Lewis acidic oxide Al_2O_3 was selected as the support. Furthermore, it should be better to make the Al_2O_3 fluffy,[43] mesoporous,[44] and amorphous.[45] First, the specific surface area and pore size can be greatly increased, which can reduce the mass transfer resistance. Second, more defects (mainly oxygen vacancies) can be created when crystallinity is destroyed. Oxygen vacancies tend to adsorb the O in oxygen-containing functional groups.[46] Moreover, the absence of O produces coordination unsaturated Al, increasing the number of empty orbitals and thus enhancing Lewis acidity, which further enhances electrophilicity.

Therefore, an Ag–In_2O_3 Schottky junction supported on fluffy mesoporous Al_2O_3 (*f-m*-Al_2O_3) was designed and synthesized for the selective hydrogenation C=O of UAL. Electron-rich Ag reduces the probability of adsorption of the C=C bond, while electron-deficient In_2O_3 improves the adsorption probability of the C=O bond. The fluffy Al_2O_3 with many electrophilic sites can also enhance the adsorption of the C=O bond, thus improving the selectivity of UAL hydrogenation to UOL. The preparation process is facile, and the catalyst cost is reduced. The combination of the Schottky effect and the fluffy structure could provide new ideas for the highly selective hydrogenation of UAL to UOL.

2. Materials and methods

2.1 Materials

P123 (the ratio of PEO : PPO : PEO = 20 : 70 : 20), γ-Al_2O_3, 1,4-dioxane, and aluminium nitrate 9-hydrate were analytically pure and purchased from Shanghai Macklin Biochemical Co., Ltd. Anhydrous ethanol, isopropyl alcohol, and cyclohexane were analytically pure and purchased from Sinopharm Chemical Reagent Co., Ltd. Anhydrous citric acid and indium nitrate hydrate were analytically pure and purchased from Shanghai Aladdin Biological Reagent Co., Ltd. Silver nitrate with the purity of 99.8% was purchased from Tianjin Tiangan Chemical Co., Ltd. All chemicals were used directly without further purification. Deionized water was used for the experiment.

2.2 Synthesis of catalysts

Preparation of *f-m*-Al_2O_3. Fluffy mesoporous Al_2O_3 was prepared by applying the hydrothermal method with P123 as a template. 1.2 g of P123 was dissolved in 30 mL of anhydrous ethanol. Then, 0.88 g of anhydrous citric acid and 3.65 g of aluminium nitrate 9-hydrate were added to the mixed solution, and the solution was stirred for 5 h until the solution was clear and uniform. The clear solution was poured into a hydrothermal kettle with a Teflon liner and heated at 90 °C for 48 h. A milky white gel solid was obtained when it was removed from the hydrothermal kettle. The white solid was washed 3 times with deionized water and then calcined at 400 °C under air for 4 h. A light yellow fluffy mesoporous Al_2O_3 solid was obtained, which is designated as *f-m*-Al_2O_3.

Preparation of catalyst Ag–In_2O_3/*f-m*-Al_2O_3. The active components of the catalyst can be evenly dispersed on the surface and within the pores of the mesoporous support through the utilization of the hydrophilic and hydrophobic properties of the support surface by applying the dual-solvent method. The preparation method was as follows: 1.0 g of *f-m*-Al_2O_3 was dispersed in 50 mL of cyclohexane and fully stirred for 3 h at room temperature. Then, a 10 mL aqueous solution of silver nitrate and indium nitrate with appropriate concentration was prepared, added dropwise into the suspension of cyclohexane and the support with stirring. After the evaporation of the solvent, the catalyst-loaded support was ground into a fine powder and calcined at 350 °C with air for 4 h. Following this, the catalyst was further reduced at 400 °C for 4 h using a 5% H_2/95%N_2 to obtain the Ag–In_2O_3/*f-m*-Al_2O_3.

2.3 Catalytic hydrogenation reaction

First, 100 mg of Ag–In_2O_3/*f-m*-Al_2O_3 and 10 mL of 0.1 mol L^{-1} reaction substrate in isopropyl alcohol solution were added to the autoclave. The reactor was replaced five times with H_2 and then charged with H_2 to 2.5 MPa. After reacting at 160 °C for 3 h, the reactor was placed into an ice bath to cool down. After

the reaction system was reduced to room temperature, the gas was released, and the reaction liquid was filtered. Conversion and selectivity were determined by GC-FID with 1,4-dioxane as an internal standard.

2.4 Characterization

Transmission electron microscopy (TEM) results were obtained by field emission transmission electron microscopy (FEI Tecnai G2 F30). High resolution transmission electron microscopy (HRTEM) was performed using a JEOL JEM-2000 EX transmission electron microscope with an accelerating voltage of 120 kV. The X-ray diffractometer used was Shimadzu's instrument (XRD-7000S), and the test conditions were as follows: the X-ray source was Al-Kα (λ = 1.542 Å), the scanning angle was 30–80°, and the scanning speed was 5° min^{-1}. The nitrogen adsorption–desorption test results were obtained at 77 K using an automatic mesoporous micropore analyzer (BK100C), and the specific surface area was calculated using the Brunauer–Emmett–Teller (BET) equation. According to the desorption data in N_2 adsorption–desorption, the pore size information of the material was calculated by applying the BJH method. The pore volume of the material is obtained, corresponding to a relative pressure P/P_0 of 0.2. XPS data were acquired by X-ray photoelectron spectroscopy (Thermo Fisher, ESCALAB 250Xi). The X-ray source is Al-Kα. Binding energy values were corrected for C 1s (284.8 eV). ICP–MS was used to determine the elemental content in the samples, which was detected by applying an inductively coupled plasma mass spectrometer (Agilent, 7900). UPS data were acquired by UV photoelectron spectroscopy (Thermo Fisher, ESCALAB 250Xi). The radiation source is a He I light source calibrated with Au. Raman data were acquired by applying a laser microscope Raman spectrometer (Thermo Fisher DXR, inVia). The instrument used for NH_3-TPD is Micromeritics AutoChem II 2920 from the United States.

3. Results and discussion

3.1 Structure, morphology, and composition

X-ray diffraction (XRD) is used to analyse the structure of the catalyst first. As shown in Fig. S2,† Al_2O_3 is an amorphous structure. The diffraction peak of In cannot be found on XRD because of the small content and good dispersion of In, but the diffraction peaks of Ag corresponding to the (111), (200), and (220) planes can be clearly observed. The Ag peaks of the catalyst doped with In are widened, which shows that the doping of In is beneficial to the dispersion of Ag.

To further understand the microstructure of the catalyst, high resolution transmission electron microscopy (HRTEM) was performed, as shown in Fig. 1. From Fig. 1a–c, it is worth noting that mesoporous Al_2O_3 appears as a fluffy structure. Compared with the conventional spherical structure, this special fluffy structure has a larger surface area and pore volume, which can improve diffusion efficiency. The active components of the catalyst supported on mesoporous Al_2O_3 are uniformly dispersed, and the particle size is about 30 nm.

As shown in Fig. 1d, the lattice spacing of 0.238 nm corresponds to the Ag (111) plane, while 0.257 nm is the lattice spacing of the In_2O_3 (400) plane. It can be observed that Ag is in close contact with In_2O_3, which agrees with the formation conditions of the Schottky junction. Fig. 1e depicts a schematic diagram of the element distribution of the Ag–-In_2O_3/*f*-*m*-Al_2O_3 catalyst. It can be observed that the active components

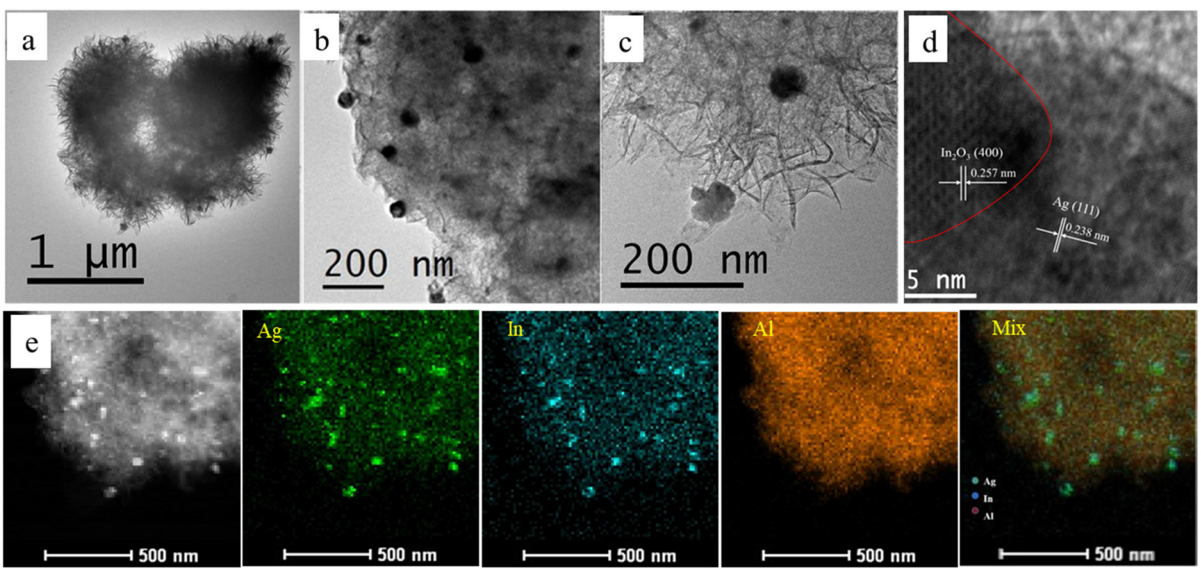

Fig. 1 (a), (b) and (c) Transmission electron microscopy images of Ag–In_2O_3/*f*-*m*-Al_2O_3 at different magnifications. (d) High resolution transmission electron microscopy image of Ag–In_2O_3/*f*-*m*-Al_2O_3. (e) STEM-HAADF image of Ag–In_2O_3/*f*-*m*-Al_2O_3 and mapping images of Ag, In, and Al elements and their overlap.

Ag and In on the catalyst are uniformly dispersed and highly overlapped.

3.2 Electron transfer and Schottky junction

X-ray photoelectron spectroscopy (XPS) was used to examine the valence state of the elements on the catalyst surface (Fig. 2). As shown in Fig. 2a, the binding energy of Ag is reduced by 0.15 eV after combination with In_2O_3, reflecting an increase in the electron density. According to the In 3d spectra (Fig. 2b), In exists as an oxidation state, and the binding energy increases by 0.10 eV upon contact with Ag, indicating that In_2O_3 has lost some electrons. This shows that electron transfer occurs from In_2O_3 to Ag, forming a metal–n-type semiconductor Schottky junction. This is very advantageous for the hydrogenation of UAL to UOL because the electron-rich Ag repels the C=C bond[31] and promotes the heterolytic of H_2.[21,22,46] Meanwhile, the electron-deficient In_2O_3 serves as an electrophilic site promoting C=O adsorption.[31]

The work function is a parameter that reflects the ability of a substance to donate or gain electrons. The larger the work function, the easier it is for the substance to gain electrons, while the smaller the work function, the easier it is for the substance to donate electrons. When a metal and semiconductor contact, electrons spontaneously flow from the side with a smaller work function to the side with a larger work function until their work functions are the same. UPS characterization is a common method for analysing the work function of substances. Knowing the change in the work function of the two materials can help us understand the direction of the electron transfer of catalysts more intuitively. As shown in Fig. S3,† the work functions of Ag/*f-m*-Al_2O_3, In_2O_3/*f-m*-Al_2O_3 and Ag–In_2O_3/*f-m*-Al_2O_3 are about 3.70 eV, 2.83 eV and 3.20 eV, respectively. It can be explained that electrons are spontaneously transferred from In_2O_3 with a smaller work function to Ag with a larger work function, which further supports the direction of electron transfer in the Ag–In_2O_3 Schottky junction.

3.3 Physical and chemical properties

Fig. 3a and b show the N_2 isothermal adsorption and desorption curves and pore size distribution of Ag–In_2O_3/*f-m*-Al_2O_3. The type IV isotherm and type H1 hysteresis loop proved that the catalyst was a typical mesoporous material. The pore size is about 5.8 nm. Table S1† shows the pore volume and specific surface area of the material. As can be observed from the table, owing to the fluffy structure of mesoporous Al_2O_3, compared with commercial Al_2O_3, the specific surface area is increased more than 10 times, and the pore volume is also increased several times, which makes the catalyst expose more active sites.

Furthermore, the fluffy structure can expose more Al unsaturated coordination sites and increase the Lewis acid content. As shown in Fig. 2c, the content of oxygen vacancy (Ov) in Ag–In_2O_3/*f-m*-Al_2O_3 (40.1%) increased significantly compared to that in Ag–In_2O_3/γ-Al_2O_3 (31.5%). Meanwhile, the binding energy of Al 2p decreased (Fig. 2d), meaning that Al has a higher electron density and thus a lower valence state, which is in accordance with the deficiency of oxygen. With the deficiency of oxygen, the degree of coordination unsaturation

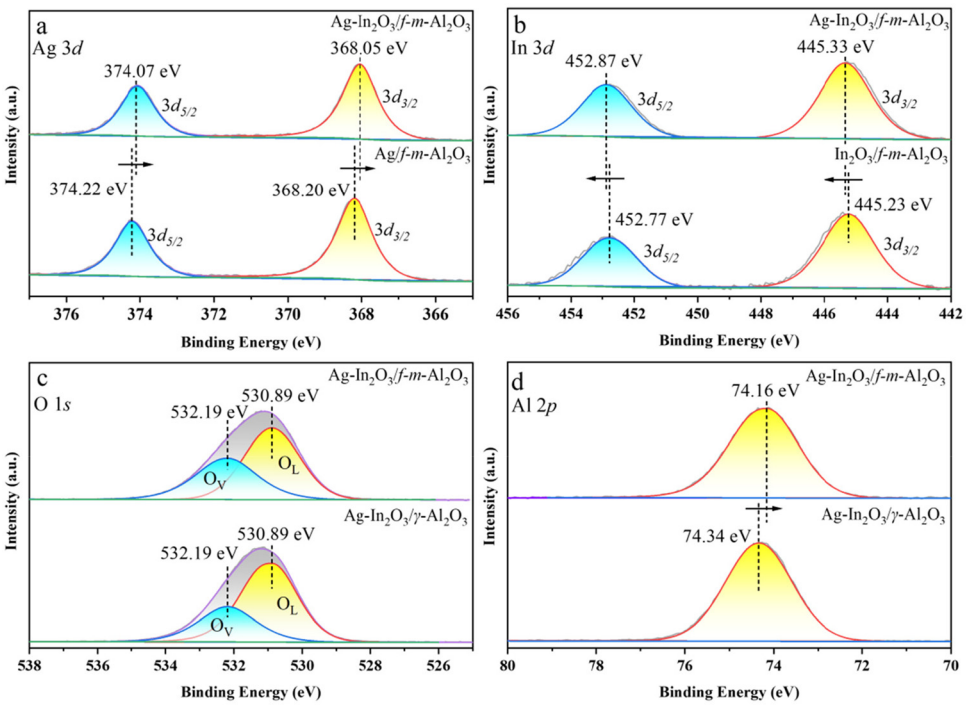

Fig. 2 XPS spectra: (a) Ag 3d spectra of Ag–In_2O_3/*f-m*-Al_2O_3 and Ag/*f-m*-Al_2O_3; (b) In 3d spectra of Ag–In_2O_3/*f-m*-Al_2O_3 and In_2O_3/*f-m*-Al_2O_3; (c) O 1s spectra of Ag–In_2O_3/*f-m*-Al_2O_3 and Ag–In_2O_3/γ-Al_2O_3; (d) Al 2p spectra of Ag–In_2O_3/*f-m*-Al_2O_3 and Ag–In_2O_3/γ-Al_2O_3.

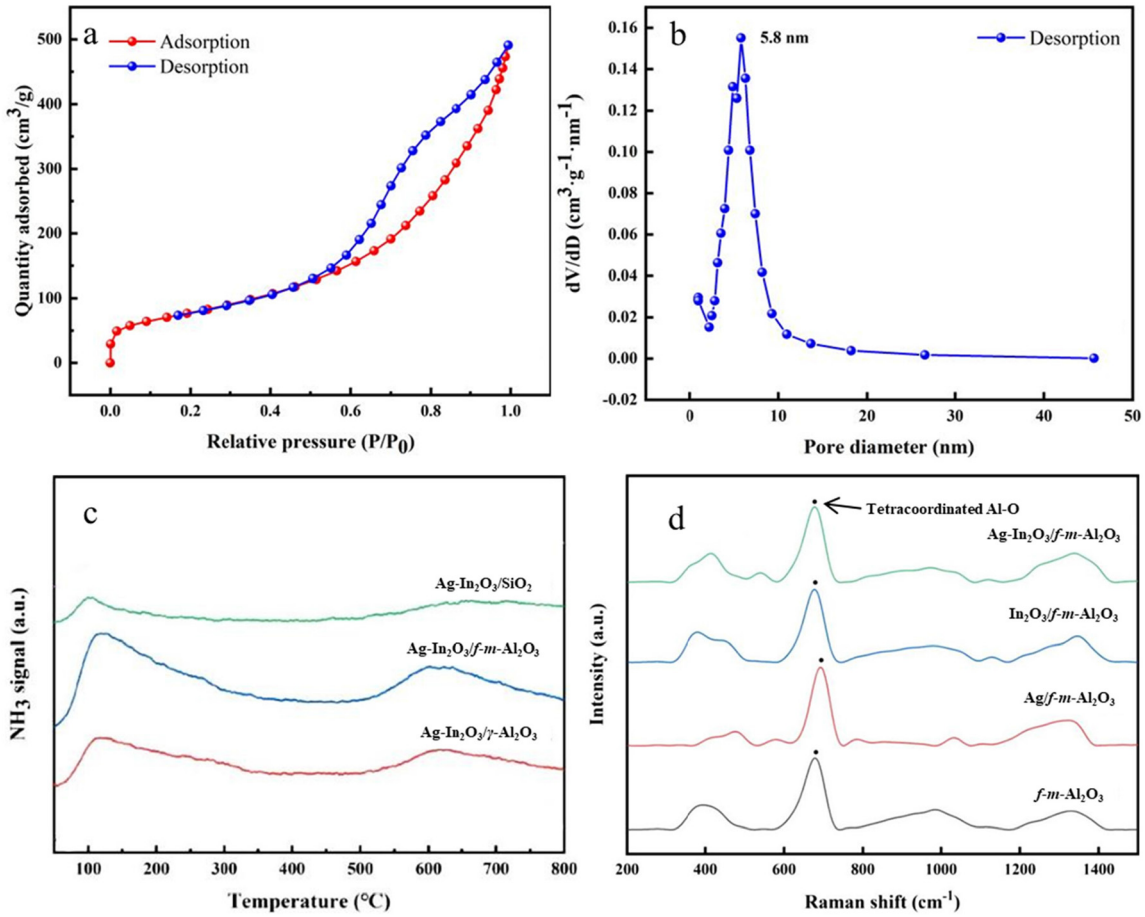

Fig. 3 (a) N_2 adsorption–desorption isotherm. (b) Pore size distribution diagram of the Ag–In_2O_3/*f-m*-Al_2O_3 catalyst. (c) NH_3-TPD of different catalysts. (d) Raman spectra for different catalysts.

of Al increases, resulting in more empty orbitals and, thus, more Lewis acidity.

To prove the increase in Lewis acidity, NH_3-TPD was used to detect the acid amounts of the different catalysts (Fig. 3c). Compared with SiO_2 and γ-Al_2O_3, self-made *f-m*-Al_2O_3 can provide more acidic sites for the catalyst, which once again shows the advantages of the fluffy structure. Lewis acid acts as an electrophilic site to adsorb a lone pair on O with C═O, so the selectivity of UOL can be further improved. Consistent with the change in acid amounts, the UOL selectivity of Ag–In_2O_3 supported on *f-m*-Al_2O_3 increased by 17% and 45% compared to those on γ-Al_2O_3 and SiO_2, respectively.

To test the degree of coordination unsaturation of Al, the catalysts were analyzed by Raman, and the results are shown in Fig. 3d. The spectral peak of 705 cm^{-1} belongs to the symmetric stretching vibration caused by four-coordinated Al–O. Because the hexa-coordinated octahedral structure of Al cannot absorb electrons, the unsaturated coordination of Al is the main reason for Lewis acidity. Raman shows that *f-m*-Al_2O_3 contains a large number of unsaturated tetra-coordinated Al–O bonds, which can be used as Lewis acid sites, further proving that the unique fluffy structure of *f-m*-Al_2O_3 can increase the number of electrophilic sites.

3.4 Catalytic performance

To test the catalytic performance of Ag–In_2O_3/*f-m*-Al_2O_3, three typical UAL, 2-pentenal, cinnamaldehyde, and furfural (representing aliphatic, aromatic and heterocyclic groups, respectively) were tested (Table 1). Notably, 98% conversion of 2-pentenal and 92% selectivity of 2-pentenol were obtained for the hydrogenation of 2-pentenal using Ag–In_2O_3/*f-m*-Al_2O_3 catalyst at 160 °C and 2.5 MPa hydrogen pressure for 3 hours. The

Table 1 Catalytic performance of the three representative UALs[a]

Entry	Substrate	Conversion (%)	Selectivity (%)
1	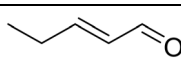	98	92
2	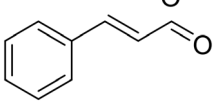	91	82
3	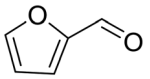	85	94

[a] Reaction conditions: substrate (1.8 mmol), catalyst (5 mol%), and isopropanol (20.0 mL) under a 2.5 MPa H_2 atmosphere at 160 °C for 3 h.

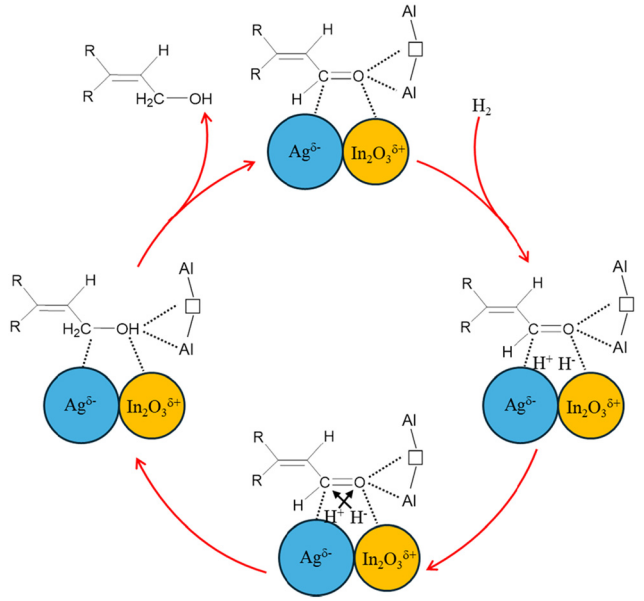

Fig. 4 The proposed mechanism for the hydrogenation of UALs to UOLs over Ag–In_2O_3/*f-m*-Al_2O_3.

other two types of UAL also have good performance. The stability test is shown in Fig. S4.† The activity can be maintained after 5 cycles, which shows that the catalyst is very stable.

Fig. 4 shows the proposed mechanism of the reaction. The electron-rich Ag repels the C=C bond while attracting the electron-deficient C in the C=O bond, and the electron-deficient indium oxide attracts the electron-rich oxygen in the C=O bond, thus achieving diσ_{CO} adsorption mode. Oxygen vacancies in the support and Lewis acid sites simultaneously help attract O in the C=O bond, further improving selectivity. H_2 is broken into active H^+ and H^- at the heterojunction interface *via* hetero cleavage and is then selectively added to the polar C=O bond to form UOL. Then, the UOL desorbs, and the catalyst recovers and enters the next cycle.

4. Conclusions

In summary, Ag–In_2O_3/*f-m*-Al_2O_3 showed high selectivity for the hydrogenation of UAL to UOL. The analysis shows that the addition of In can regulate the electronic distribution of the catalyst. A Schottky junction can be formed between Ag and In_2O_3. Because of the larger work function of Ag, electrons flow from In_2O_3 to Ag. Electron-rich Ag reduces the probability of adsorption of the C=C bond owing to the "four-electron repulsion" effect. Electron-deficient In_2O_3 can increase the probability of C=O bond adsorption. Furthermore, the unsaturated coordination of Al–O in *f-m*-Al_2O_3 not only improves the selectivity of the C=O bond by generating electrophilic sites, such as the oxygen vacancy and Lewis acid site, but also increases the specific surface area of the catalyst and reduces the mass transfer resistance. High selectivity of UOL can be obtained from UAL containing aliphatic, aromatic and heterocyclic groups. The design of this catalyst is expected to provide a new idea for achieving highly selective hydrogenation of UALs to UOLs.

Author contributions

Jiasheng Wang: conceptualization, supervision, funding acquisition, and Writing–review and editing. Tianyu Zhang and Fengxin Zhang: investigation and Writing–original draft. Jiliang Song and Hong Liu: methodology. Wan-Hui Wang and Ming Bao: resources and Supervision.

Data availability

The data supporting this article have been included as part of the ESI.†

Conflicts of interest

There are no conflicts to declare.

Acknowledgements

We acknowledge the financial support by the National Natural Science Foundation of China (22278063) and the Research and Innovation Team Project of Dalian University of Technology (DUT2022TB10).

References

1 Q. Liu, Q. Liu, Y. Chen, Y. Li, H. Su, Q. Liu and G. Li, *Chin. Chem. Lett.*, 2022, **33**, 374–377.
2 X. Wang, X. Liang, P. Geng and Q. Li, *ACS Catal.*, 2020, **10**, 2395–2412.
3 H. Yu, J. Zhao, C. Wu, B. Yan, S. Zhao, H. Yin and S. Zhou, *Langmuir*, 2021, **37**, 1894–1901.
4 S. Zhou, Y. Yang, T. Shen, P. Yin, L. Wang, Z. Ren, L. Zheng, B. Wang, H. Yan and M. Wei, *ACS Appl. Mater. Interfaces*, 2024, **16**, 13685–13696.
5 Q. Liu, J. Wu, J. Kang, Q. Liu, P. Liao and G. Li, *Nanoscale*, 2022, **14**, 15462–15467.
6 Y. Wang, P. Wang, M. Zhang, X. Yi, Y. Wei and J. Zhu, *Fine Chem.*, 2024, **41**, 1581–1589.
7 X. Lan and T. Wang, *ACS Catal.*, 2020, **10**, 2764–2790.
8 N. Luo, J. Liao, L. Ouyang, H. Wen, J. Liu, W. Tang and R. Luo, *Organometallics*, 2019, **38**, 3025–3031.
9 C. A. Barrales-Cortés, H. Pérez-Pastenes, J. C. Piña-Victoria and T. Viveros-García, *Top. Catal.*, 2020, **63**, 468–480.
10 Z. Gao, L. Cai, C. Miao, T. Hui, Q. Wang, D. Li and J. Feng, *ChemCatChem*, 2022, **14**, e202200634.
11 M. Luneau, J. S. Lim, D. A. Patel, E. C. H. Sykes, C. M. Friend and P. Sautet, *Chem. Rev.*, 2020, **120**, 12834–12872.

12 Y. Liang, J. He, Y. An, J. Zhang, G.-S. Park, L. Zhao, R. Oh, X. Huang, J. Dong and L. Liu, *Chem. Eng. J.*, 2024, **484**, 149670.
13 P. Adamski, H. Zhang, S. Kaur, X. Chen, C. Liang and M. Armbrüster, *Chem. Mater.*, 2024, **36**, 10383–10407.
14 F. Delbecq and P. Sautet, *J. Catal.*, 1995, **152**, 217–236.
15 F. Delbecq and P. Sautet, *J. Catal.*, 2002, **211**, 398–406.
16 L. Zhong, X. Liao, H. Cui, J. Huang, H. a. Luo, Y. Lv and P. Liu, *ACS Catal.*, 2024, **14**, 15799–15810.
17 Z. Tian, L. Wang, T. Shen, P. Yin, W. Da, Z. Qian, X. Zhao, G. Wang, Y. Yang and M. Wei, *Chem. Eng. J.*, 2023, **472**, 144876.
18 L. Zhong, X. Liao, H. Cui, H. a. Luo, Y. Lv and P. Liu, *ACS Catal.*, 2024, **14**, 857–873.
19 K. K. Ghuman, L. B. Hoch, P. Szymanski, J. Y. Y. Loh, N. P. Kherani, M. A. El-Sayed, G. A. Ozin and C. V. Singh, *J. Am. Chem. Soc.*, 2016, **138**, 1206–1214.
20 X. Deng, B. Qin, R. Liu, X. Qin, W. Dai, G. Wu, N. Guan, D. Ma and L. Li, *J. Am. Chem. Soc.*, 2021, **143**, 20898–20906.
21 J. Wang, H. Jin, W.-H. Wang, Y. Zhao, Y. Li and M. Bao, *ACS Appl. Mater. Interfaces*, 2020, **12**, 19581–19586.
22 X. Xu, N. Luo, W.-H. Wang, M. Bao and J. Wang, *ACS Appl. Mater. Interfaces*, 2024, **16**, 70489–70497.
23 Q. Liu, J. Xian, Y. Li, Q. Zhang, H. Kitagawa and G. Li, *CCS Chem.*, 2022, **4**, 3275–3284.
24 W. Yang, Q. Liu, J. Yang, J. Xian, Y. Li, G. Li and C.-Y. Su, *CCS Chem.*, 2022, **4**, 2276–2285.
25 Y. Chen, X. He, L. Hou, B. Liu, L. Dong and X. Ge, *Chem. Eng. J.*, 2024, **500**, 156934.
26 H. Wang, S. Bai, Y. Pi, Q. Shao, Y. Tan and X. Huang, *ACS Catal.*, 2019, **9**, 154–159.
27 Y. Zhong, P. Liao, J. Kang, Q. Liu, S. Wang, S. Li, X. Liu and G. Li, *J. Am. Chem. Soc.*, 2023, **145**, 4659–4666.
28 J. Xian, S. Li, H. Su, P. Liao, S. Wang, Y. Zhang, W. Yang, J. Yang, Y. Sun, Y. Jia, Q. Liu, Q. Liu and G. Li, *Angew. Chem., Int. Ed.*, 2023, **62**, e202304007.
29 X.-H. Li and M. Antonietti, *Chem. Soc. Rev.*, 2013, **42**, 6593–6604.
30 J. Michel, D. Splith, J. Rombach, A. Papadogianni, T. Berthold, S. Krischok, M. Grundmann, O. Bierwagen, H. von Wenckstern and M. Himmerlich, *ACS Appl. Mater. Interfaces*, 2019, **11**, 27073–27087.
31 M. Deng, D. Wang and Y. Li, *Appl. Catal., A*, 2023, **666**, 119423.
32 Y. Ma, D. He, Z. Hu, H. Li and X. Wang, *J. Phys. Chem. C*, 2024, **128**, 5064–5074.
33 C. Wang, Z. Zhao, Y. Peng, L. Ma, X. Liu, F. Fu and Y. Wu, *Fuel*, 2024, **372**, 132231.
34 Y. Ren, H. Xu, B. Han and J. Xu, *Molecules*, 2023, **28**, 4136.
35 Z. Yin, F. Yang, J. Chen, C. Sun and S. Cao, *Appl. Catal., A*, 2022, **644**, 118807.
36 E. Plessers, D. E. De Vos and M. B. J. Roeffaers, *J. Catal.*, 2016, **340**, 136–143.
37 X. Yang, A. Wang, X. Wang, T. Zhang, K. Han and J. Li, *J. Phys. Chem. C*, 2009, **113**, 20918–20926.
38 L. Tian, Q. Yang, Z. Jiang, Y. Zhu, Y. Pei, M. Qiao and K. Fan, *Chem. Commun.*, 2011, **47**, 6168–6170.
39 Y. Hinuma, T. Toyao, N. Hamamoto, M. Takao, K.-i. Shimizu and T. Kamachi, *J. Phys. Chem. C*, 2020, **124**, 27621–27630.
40 J. Jin, C. Liu, C. Dai, C. Zeng, Y. Jia and X. Liu, *Environ. Res.*, 2024, **251**, 118649.
41 Y. Zhang, S. Zhang, X. Pan, M. Bao, J. Huang and W. Shen, *Catal. Lett.*, 2017, **147**, 102–109.
42 Y. Wang, S. Wang, Q. Xu, X. Feng, W. Liu, Y. Yamamoto, Y. Shi and M. Bao, *ACS Appl. Nano Mater.*, 2024, **7**, 10739–10747.
43 J. Zhu, S. Yan, Y. Qian, X. Zhu and F. Yang, *Microporous Mesoporous Mater.*, 2023, **351**, 112465.
44 F. Ebert, P. Ingale, S. Vogl, S. Praetz, C. Schlesiger, N. Pfister, R. N. d'Alnoncourt, B. R. Cuenya, A. Thomas, E. Gioria and F. Rosowski, *ACS Catal.*, 2024, **14**, 9993–10008.
45 S. Arora, R. Khan and S. Sivakumar, *ChemCatChem*, 2025, **17**, e202401673.
46 J. Wang, Y. Zhang, X. Xu and M. Bao, *ACS Appl. Mater. Interfaces*, 2023, **15**, 8149–8156.